Applied Catalysis B: Environmental 327 (2023) 122437

Contents lists available at ScienceDirect

Applied Catalysis B: Environmental

journal homepage: www.elsevier.com/locate/apcatb

Silica modulated palladium catalyst with superior activity for the selective catalytic reduction of nitrogen oxides with hydrogen

Shaohua Xie [a], Yuejin Li [b], Chunying Wang [c], Ke-Bin Low [b], Kailong Ye [a], Daekun Kim [a], Xing Zhang [a], Yaobin Li [c], Yan Zhang [c], Fengyuan Shi [d], Lu Ma [e], Steven N. Ehrlich [e], Fudong Liu [a,*]

[a] Department of Civil, Environmental, and Construction Engineering, Catalysis Cluster for Renewable Energy and Chemical Transformations (REACT), NanoScience Technology Center (NSTC), University of Central Florida, Orlando, FL 32816, United States
[b] BASF Corporation, Iselin, NJ 08830, United States
[c] Center for Excellence in Regional Atmospheric Environment, Institute of Urban Environment, Chinese Academy of Sciences, Xiamen 361021, China
[d] Electron Microscopy Core, Research Resources Center, University of Illinois Chicago, Chicago, IL 60607, United States
[e] National Synchrotron Light Source II (NSLS-II), Brookhaven National Laboratory, Upton, NY 11973, United States

ARTICLE INFO

Keywords:
Palladium catalyst
SiO_2 modification
H_2-SCR
H_2 dissociation
Bridging bidentate nitrates

ABSTRACT

A significant promotion effect of colloidal SiO_2 on Pd/TiO_2 catalyst for improving the activity and N_2 selectivity in the selective catalytic reduction of NO with H_2 (H_2-SCR) was reported, both before and after hydrothermal aging. The SiO_2 addition not only benefited the formation of more oxygen vacancies but also increased Pd dispersion and created rich Pd-SiO_2 interfaces on Pd-SiO_2/TiO_2 catalyst. The H_2-SCR of NO on both Pd/TiO_2 and Pd-SiO_2/TiO_2 followed a Langmuir-Hinshelwood mechanism, in which the adsorbed bridging bidentate nitrates on TiO_2 could react with dissociated H_2 species on Pd sites at Pd-TiO_2 interface. Particularly, on the promoted Pd-SiO_2/TiO_2, the Pd-TiO_2 interface could facilitate NO adsorption and activation, and the created Pd-SiO_2 interface could benefit H_2 adsorption and dissociation, thus contributing to its significantly improved H_2-SCR activity. Furthermore, the active Pd species (which should be Pd^0 under reaction condition with higher surface concentration) within Pd-SiO_2/TiO_2 could be well stabilized during long-term hydrothermal aging process through the formation of rich Pd-SiO_2 interfaces.

1. Introduction

With the growing concern of climate change, strategies for reducing carbon emissions are in urgent requirement, particularly in the transportation area. On the way toward net zero of carbon emissions from vehicles, one of the most promising strategies will be using hydrogen (H_2) as a carbon-free fuel for lean-burn internal combustion engines (ICE). To meet the tightening vehicle emission regulations worldwide at the same time, efficient exhaust aftertreatment systems for lean-burn ICE are highly demanded especially for the removal of nitrogen oxides (NO_x). Selective catalytic reduction (SCR) of NO_x is one of the most efficient and widely used technologies to control NO_x emissions from engine exhausts in excess oxygen. Comparing to the involvement of NH_3 as reducing agent showing secondary pollution concern in the NH_3-SCR of NO_x, for H_2-ICE application, the environmentally benign H_2 from the fuel tank can be directly used as reducing agent for the H_2-SCR of NO_x [1–3]. The key issue to be solved for the broad application of H_2-SCR technology is the development of robust H_2-SCR catalyst which can operate at low temperatures, exhibit high hydrothermal stability and achieve the low formation of N_2O byproduct (which is a strong greenhouse gas).

It has been reported that supported noble metal (*e.g.*, Pt, Pd, Rh, Ir) catalysts are promising for the H_2-SCR reaction [2,4–10]. In particular, the supported Pd catalysts usually show broad operation temperature window and high N_2 selectivity (*i.e.*, low N_2O yield) during the H_2-SCR of NO_x [11,12]. However, these advantages for Pd catalysts are balanced with the low NO_x reduction activity at low temperatures such as below 150 °C [13,14]. Therefore, many efforts have been devoted to the improvement of low temperature DeNO_x activity of Pd-based catalysts, [2,3,14,15] which mainly focused on the modulation of Pd states by varying the distinct supports and promoters. It was found that the H_2-SCR performance of Pd catalysts was highly dependent on the

* Corresponding author.
E-mail address: fudong.liu@ucf.edu (F. Liu).

https://doi.org/10.1016/j.apcatb.2023.122437
Received 28 October 2022; Received in revised form 3 December 2022; Accepted 4 February 2023
Available online 7 February 2023

reducibility of supports. For example, by tuning the redox ability of CeO_2 with Al_2O_3, ZrO_2, MgO and TiO_2 doping, the low-temperature H_2-SCR activity on Pd/CeO_2 can be greatly improved [16]. Comparing to Pd/CeO_2 reference catalyst, the Pd/ZrO_2-CeO_2 catalyst showed higher H_2-SCR activity within a wide temperature range (100–400 ℃) with relatively high N_2 selectivity [16]. Qing et al. reported that acidic SiO_2 was a superior support for Pd catalyst when comparing to MgO and Al_2O_3 supports in H_2-SCR reaction due to the enhanced formation of NH_x intermediates on Pd/SiO_2 catalyst [17].

Besides of tuning the support property, creating Pd-metal or Pd-metal oxide interface also showed great benefits on improving the H_2-SCR activity [18–24]. For instance, by modifying Pd using other noble metals such as Au and Ir, the Pd-Au or Pd-Ir interface could be created, which led to the significant improvement of H_2-SCR activity on Pd/TiO_2 catalyst [19,20,25]. Hu et al. also reported the promotional effects of Fe, Co, Cu and Ni modification on the H_2-SCR performance of Pd/TiO_2 [21, 22]. It was concluded that the synergistic effects between Pd and transition metals (*i.e.*, Fe, Co, Cu and Ni) enhanced the migration distance and intrinsic rate of hydrogen spillover, which facilitated more formation of active monodentate nitrates and extra NH_x species as reaction intermediate, thus contributing to the significant enhancement of H_2-SCR activity on Pd/TiO_2 [22]. It was also reported that the addition of Ni and Sn into Pd/TiO_2-Al_2O_3 catalyst facilitated the oxidation of NO to NO_2 and the absorption of NO_x, which played important roles in the H_2-SCR of NO_x [23]. Duan et al. concluded that the addition of Mn not only enhanced the H_2-SCR activity but also remarkably increased the N_2 selectivity (above 150 °C) on Pd/TiO_2-Al_2O_3 catalyst [24]. It was demonstrated that the Mn modification promoted the adsorption and activation of NO on Pd/TiO_2-Al_2O_3 catalyst due to the synergetic effect between Pd and Mn. Although great efforts have been made on enhancing the H_2-SCR performance over Pd catalysts especially in fresh state, few works reported the improvement of N_2 selectivity, the hydrothermal aging effect on H_2-SCR catalysts and the use of testing conditions close to practical applications. Moreover, the inferior H_2-SCR activity of Pd-based catalysts at low temperatures still requires further improvement to meet the stringent $DeNO_x$ requirements for practical applications.

In this work, we report a significant promotion effect of colloidal SiO_2 on the H_2-SCR performance of Pd/TiO_2 catalyst. The facile synthesis of Pd-SiO_2/TiO_2 catalyst using co-incipient wetness impregnation (co-IWI) method and colloidal SiO_2 as precursor was not only novel but also beneficial for potential scale-up in practical applications. With the modification by SiO_2, both the H_2-SCR activity and N_2 selectivity on Pd-SiO_2/TiO_2 catalyst were largely enhanced not only before but also after hydrothermal aging. Through systematic characterizations using scanning transmission electron microscopy (STEM), X-ray absorption spectroscopy (XAS), X-ray photoelectron spectroscopy (XPS), hydrogen-temperature programmed reduction (H_2-TPR), *in situ* diffuse reflectance infrared Fourier transform spectroscopy (*in situ* DRIFTS) and kinetic studies, the effect of SiO_2 modification on the structure and H_2-SCR mechanism over Pd-SiO_2/TiO_2 catalyst has been clearly revealed. It was demonstrated that creating functional Pd-metal oxide interfaces, including Pd-SiO_2 and Pd-TiO_2 interfaces, was an effective strategy to improve the H_2-SCR performance and hydrothermal stability of Pd catalyst.

2. Experimental section

2.1. Materials

Commercial TiO_2 in anatase phase (with specific surface area as *ca.* 90 m^2/g) was obtained from Tronox Inc. Colloidal SiO_2 with average size of 12 nm were received from W. R. Grace & Co. Palladium nitrate was purchased from Umicore Precious Metals Chemistry, LLC. 10 % H_2/Ar, 1 % NO/N_2, 1 % NH_3/N_2, CO_2 (99.99 %), O_2 (99.999 %) and Ar (99.999 %) gas cylinders were purchased from Airgas. No further treatment was conducted on all chemicals and cylinders used in this work.

2.2. Catalyst preparation

The Pd-SiO_2/TiO_2 catalysts with x wt% of SiO_2 loadings ($x = 0$, 3, 5, 8 or 10) were prepared by co-IWI method using colloidal SiO_2 as precursor. Typically, a mixed solution of palladium nitrate (1 wt% Pd) and colloidal SiO_2 with determined concentration was added dropwise onto commercial TiO_2 support under stirring and then dried at 120 °C for 1 h. After calcination in air at 550 °C for 2 h with a temperature ramp of 5 °C/min, the catalysts with different SiO_2 loadings were obtained and denoted as Pd-$x$$SiO_2$/$TiO_2$. The Pd-8$SiO_2$/$TiO_2$ catalyst performed the best for the H_2-SCR of NO_x in this work, which was denoted as Pd-SiO_2/TiO_2 for detailed study. To simulate the application conditions on heavy-duty diesel vehicles, all aged catalysts were obtained by treating the samples in a flow of 10 % H_2O and 10 % O_2 at 650 °C for 50 h, and labeled with '-Aged'.

2.3. Catalyst characterizations

X-ray powder diffraction (XRD) patterns were collected on a PANalytical Empyrean diffractometer using a Cu Kα X-rays ($\lambda = 0.15406$ nm). The range of XRD patterns was 10–80 ° and the scan speed was 6 °/min with a scan step of 0.067°.

Nitrogen (N_2) adsorption-desorption isotherm analysis was performed on a Quantachrome Autosorb-iQ physisorption chemisorption instrument. Measurements were performed at 77 K using liquid N_2 bath. Prior to testing, the samples were outgassed at 300 °C for 1 h to remove all adsorbed molecules from the surface, and the N_2 adsorption-desorption isotherm was measured using pressure intervals of $0 < P/P_0 < 1$ with 20 adsorption steps and 20 desorption steps.

High-angle annular dark-field scanning transmission electron microscopy (HAADF-STEM) was performed on a cold field emission STEM (JEOL JEM-ARM200CF) using a nominal probe size and current of about 0.1 nm and 60 pA as well as dark field signal collection semi-angle ranges between 90 and 370 mrad, and a transmission electron microscope (FEI Tecnai F30 TEM) with HAADF/ADF/BF STEM and EDS detectors at 200 kV. The energy dispersive X-ray spectroscopy (EDS) mapping images were collected on the FEI Tecnai F30 TEM.

X-ray photoelectron spectroscopy (XPS, VG CLAM 4 MCD analyzer) was used to determine the binding energies (BEs) of O 1s, Pd 3d and C 1s for surface species on all catalysts using Mg K-α ($h\nu = 1253.6$ eV) as an excitation source. The catalysts were degassed in the preparation chamber (10^{-5} Torr) for 0.5 h and then introduced into the analysis chamber (3×10^{-9} Torr) for XPS recording. The C 1s signal at 284.6 eV was taken as a reference for BE calibration.

X-ray absorption near edge structure (XANES) and extended X-ray absorption fine structure (EXAFS) of Pd K-edge were measured in fluorescent mode at room temperature at beamline 7-BM QAS of the National Synchrotron Light Source II (NSLS-II), Brookhaven National Laboratory. Data were analyzed using Athena and Artemis from the Demeter software package. A Pd foil was measured during data collection for energy calibration and drift correction of the monochromator. The processed EXAFS, $\chi(k)$, was weighted by k^2 to amplify the high-k oscillations. For Fourier-transformed (FT) spectra, the k range between 3.0 and 12.0 $Å^{-1}$ was used, and the fitting in the R range was between 1.0 and 3.2 Å in Artemis software.

Cryogenic H_2-TPR was performed on a Micromeritics AutoChem II 2920 apparatus. Prior to each testing, the catalyst was pretreated by 10 % O_2/He at 300 °C for 0.5 h followed by He purge at 25 °C for 0.5 h. After cooling down to −50 °C in He flow, the catalyst was exposed to a flow of 10 % H_2/Ar (40 mL/min) and heated from −50–700 °C at the temperature ramp of 10 °C/min. The alteration in H_2 concentration in the effluent was monitored online by a thermal conductivity detector (TCD).

NH_3 and NO-temperature programmed desorption (NH_3-TPD and NO-TPD) were conducted on a continuous flow fixed-bed quartz tubular microreactor (internal diameter = 4.0 mm). 40 mg of the catalyst (40–60 mesh) was diluted with 0.25 g of inert SiC (40–60 mesh). Prior to testing, the catalyst was pretreated in 10 % O_2/Ar flow of 50 mL/min at 300 °C for 1 h. Afterwards, the catalyst was pre-saturated in 1 % NH_3/N_2 flow or 1 % NO/N_2 flow at 50 °C for 1 h. After Ar purge for 2 h, the desorption was performed in Ar flow with temperature increased from 50 to 650 °C with the temperature ramp of 10 °C/min. The alteration in NH_3 and NO concentrations in the effluent was monitored online by a Mass Spectrometer (MS, HPR20 R&D, Hiden Analytical). The *m/z* ratios used for NH_3 and NO detection were 15 and 30, respectively.

In situ DRIFTS experiments were carried out on a Thermo Nicolet iS50 FTIR spectrometer with a liquid nitrogen-cooling MCT detector. The infrared (IR) spectra were recorded by accumulating 100 scans at a spectral resolution of 4 cm^{-1}. Before *in situ* DRIFTS experiment, 20 mg catalyst was loaded into a high temperature IR cell (PIKE DiffusIR cell with ZnSe windows), followed by a treatment in 10 % O_2/Ar flow (30 mL/min) at 300 °C for 1 h. For *in situ* DRIFTS of NH_3 adsorption/desorption experiments, background spectra were collected in flowing Ar when the powder catalyst reached target temperatures (*i.e.*, 50, 100, 150, 200, 250, and 300 °C). NH_3 adsorption was performed on the catalyst at 50 °C in the flow of 500 ppm NH_3 for 0.5 h. Then, the catalyst was purged by Ar for 0.5 h until the IR signals stabilized. Afterwards, the desorption experiments were carried out in Ar flow with the temperature increased from 50° to 300°C. The *in situ* DRIFTS of transient reactions on the catalysts at 150 °C were also performed. The reaction conditions were controlled as follows: 500 ppm NO + 1 % H_2 + 10 % O_2 (Step 1), 500 ppm NO + 10 % O_2 (Step 2), 500 ppm NO + 1 % H_2 + 10 % O_2 (Step 3), 500 ppm NO + 1 % H_2 (Step 4), 500 ppm NO + 1 % H_2 + 10 % O_2 (Step 5), using Ar as balance, and the total flow rate was100 mL/min. For each transient reaction experiment, the Step 1 was controlled for 1 h, and all other steps were controlled for 0.5 h. The IR spectra were collected continuously during the whole procedures.

2.4. Catalytic performance evaluation

Catalytic activity evaluation for the H_2-SCR of NO_x over all catalysts was carried out on a continuous flow fixed-bed quartz tubular microreactor (internal diameter = 4.0 mm). In each test, 26 mg of the catalyst (40–60 mesh) was diluted with 0.25 g of inert SiC (40–60 mesh) to minimize the effect of hot spots. The reactant mixture was composed of 500 ppm NO, 1 % H_2, 10 % O_2, 5 % CO_2 (when used) and 5 % H_2O (when used), using Ar as balance, and the total flow rate was 200 mL/min, thus giving a weight hourly space velocity (WHSV) of 461,540 $mL{\cdot}g^{-1}{\cdot}h^{-1}$ and a gas hourly space velocity (GHSV) of 565,335 h^{-1}. In the case of H_2-SCR activity test with water vapor, 5 % H_2O was introduced by passing Ar through a water saturator at 80 °C. The addition of 5 % CO_2 was always accompanied with the addition of 5 % H_2O. Reactants and products were analyzed online by a MultiGas 2030 CEMCert FTIR spectrometer coupled with MS. The *m/z* ratios used for O_2 and H_2 detection were 32 and 2, respectively. The reactant conversion was defined as $(c_{inlet} - c_{outlet})/c_{inlet} \times 100$ %, where c_{inlet} and c_{outlet} were the inlet and outlet NO_x/H_2 concentrations in the feed stream, respectively. The N_2 selectivity was defined as $([NO]_{inlet} + [NO_2]_{inlet} - [NO]_{outlet} - [NO_2]_{outlet} - 2 \times [N_2O]_{outlet})/([NO]_{inlet} + [NO_2]_{inlet} - [NO]_{outlet} - [NO_2]_{outlet}) \times 100$ %. The N_2O yield was defined as $2 \times [N_2O]_{outlet}/([NO]_{inlet} + [NO_2]_{inlet}) \times 100$ %. The N_2O selectivity was defined as $2 \times [N_2O]_{outlet}/([NO]_{inlet} + [NO_2]_{inlet} - [NO]_{outlet} - [NO_2]_{outlet}) \times 100$ %. To avoid the significant heat or mass transfer limitation, kinetic study was performed at 120 °C and WHSV of 2400,000 $mL{\cdot}g^{-1}{\cdot}h^{-1}$ for the determination of NO, H_2, O_2 and H_2O reaction orders on Pd/TiO_2-Aged and Pd-SiO_2/TiO_2-Aged catalysts.

3. Results and discussion

3.1. H_2-SCR performance on SiO_2 modified Pd/TiO_2 catalysts

Fig. S1 shows the H_2-SCR performance on SiO_2 modified Pd/TiO_2 catalysts after hydrothermal aging. With the increase of SiO_2 loading, the H_2-SCR activity on aged Pd-*x*SiO_2/TiO_2 catalysts initially increased and then decreased, which achieved the highest level when the SiO_2 loading was controlled at 8 wt% (Fig. S1A). In the meantime, due to the presence of SiO_2 promoter, the N_2 selectivity increased and the N_2O selectivity/yield declined on Pd-*x*SiO_2/TiO_2-Aged comparing to the Pd/TiO_2-Aged counterpart (Fig. S1B and S1C). For better comparison to the reported H_2-SCR catalysts in literature, the NO_x conversions and reaction rates at 150 °C were calculated and listed in Table S1. It can be clearly seen that the NO_x conversion or the H_2-SCR reaction rate at 150 °C on Pd-8SiO_2/TiO_2-Aged catalyst was *ca.* 2.8 times of that on Pd/TiO_2-Aged catalyst. Moreover, even after hydrothermal aging and under the testing conditions with both H_2O and CO_2, the Pd-8SiO_2/TiO_2-Aged catalyst developed in this work still outperformed most of the recently reported fresh Pd catalysts including 1Pd-5Ni/TiO_2,[22] $Pd_{0.5}Mn_2$/TiO_2-Al_2O_3,[24] 2 % Pd-0.5 % Au/TiO_2,[25] Pd-Ir/TiO_2, [19] and $LaFe_{0.95-x}Co_xPd_{0.05}O_3$ [26] (Table S1). For following study, the optimal Pd-8SiO_2/TiO_2 catalyst was simply denoted as Pd-SiO_2/TiO_2.

To study the hydrothermal stability, the H_2-SCR performance on Pd/TiO_2 and Pd-SiO_2/TiO_2 catalysts before and after aging was evaluated, and the results are shown in Fig. 1. Similar to the above-mentioned observation on Pd-SiO_2/TiO_2-Aged and Pd/TiO_2-Aged catalysts, the fresh Pd-SiO_2/TiO_2 catalyst also outperformed Pd/TiO_2 catalyst for the H_2-SCR reaction, with higher NO_x and H_2 conversions achieved on the former (Fig. 1A and B). It is noteworthy that hydrothermal aging resulted in an obvious decrease of DeNO_x activity and N_2 selectivity simultaneously on Pd/TiO_2 catalyst, yet no apparent change of NO_x removal efficiency and a surprisingly enhanced N_2 selectivity were observed at the same time on Pd-SiO_2/TiO_2 catalyst after aging (Fig. 1A and C). It should be highlighted that the N_2O yield decreased on both catalysts after hydrothermal aging, and the H_2-SCR reaction on Pd-SiO_2/TiO_2-Aged catalyst showed much lower N_2O yield than that on Pd/TiO_2-Aged catalyst in the range of 175–275 °C (Fig. 1D). These results clearly demonstrated that the Pd-SiO_2/TiO_2 catalyst was not only more robust but also more selective than the Pd/TiO_2 counterpart, indicating that the colloidal SiO_2 promoter could effectively boost and stabilize the Pd species within Pd-SiO_2/TiO_2 even after long-term hydrothermal aging for 50 h. The Pd-SiO_2/TiO_2-Aged catalyst could achieve the N_2 selectivity higher than 75 % in the whole temperature range investigated, which showed great potential in practical application although more efforts should be devoted to further increasing the N_2 selectivity in future study.

3.2. Structure characterization of SiO_2 modified Pd/TiO_2 catalysts

XRD technique was used to characterize the crystal structure of the fresh and aged catalysts. As shown in Fig. 2, all catalysts showed XRD patterns that could be attributed to anatase TiO_2 crystal phase. A small diffraction peak centered at 34° was observed on all Pd-containing catalysts, suggesting the presence of PdO particles with long-range ordered structure. Barely any SiO_2 phase could be detected on both fresh and aged Pd-SiO_2/TiO_2 catalysts probably due to the low loading and high dispersion of nanosized SiO_2. To reveal the effects of SiO_2 addition and hydrothermal aging on the structure of TiO_2, the grain size of TiO_2 within all catalysts was calculated according to the Scherrer equation ($D = \lambda/(\beta \cos\theta$, where λ is the X-ray wavelength, β is the full width at half maximum (FWHM) of the (101) plane of TiO_2, and θ is the corresponding diffraction angle). As the inserted values shown in Fig. 2 (also listed in Table 1), the fresh Pd/TiO_2 and Pd-SiO_2/TiO_2 catalysts showed similar grain sizes of TiO_2 crystallite (19.8 and 19.4 nm, respectively) to that of pristine TiO_2 support (19.3 nm), indicating that there was no

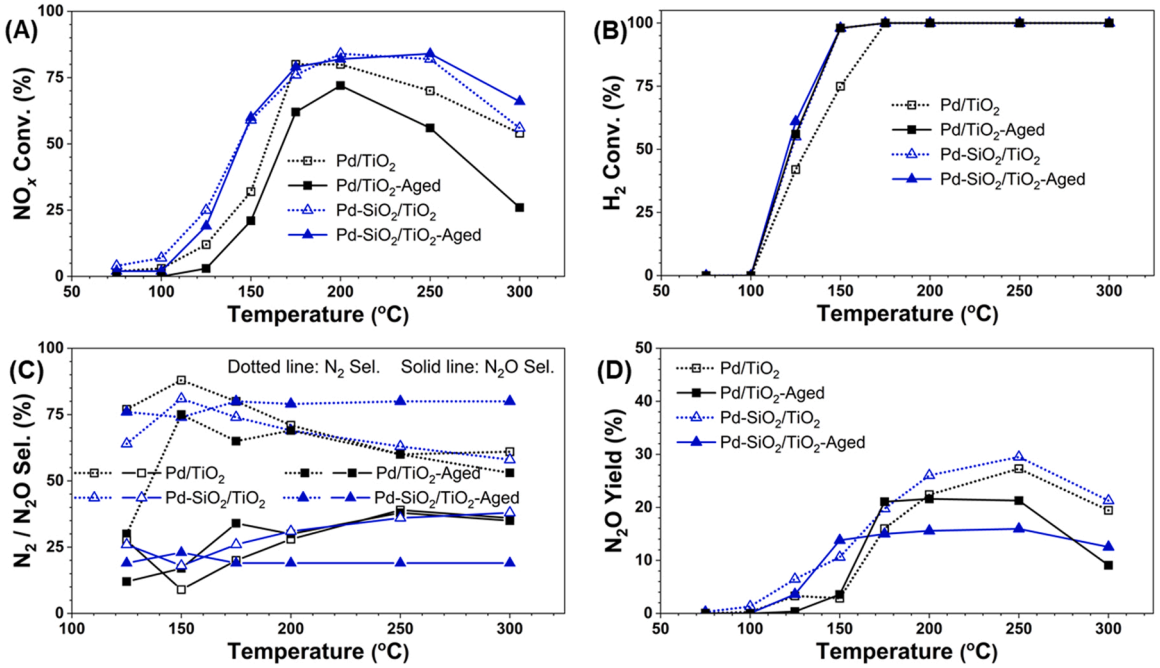

Fig. 1. Hydrothermal aging effect on H_2-SCR performance of Pd/TiO_2 and $Pd\text{-}SiO_2/TiO_2$ catalysts. (A) NO_x conversion, (B) H_2 conversion, (C) N_2/N_2O selectivity, and (D) N_2O yield as a function of reaction temperature. Reaction conditions: 500 ppm NO, 1 % H_2, 10 % O_2, 5 % CO_2 + 5 % H_2O, using Ar as balance, WHSV = 461,540 $mL{\cdot}g^{-1}{\cdot}h^{-1}$ (GHSV = 565,335 h^{-1}).

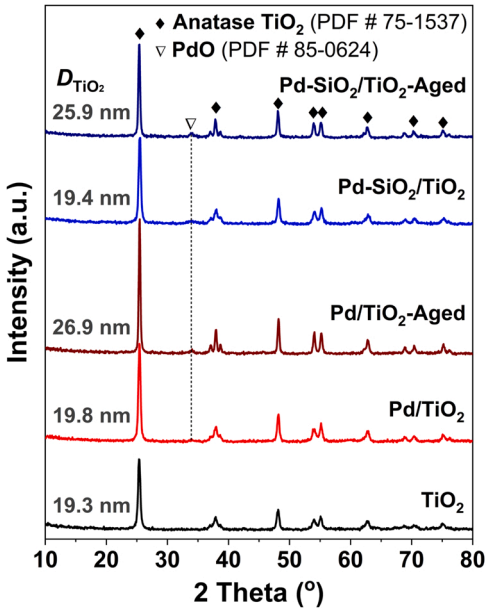

Fig. 2. XRD patterns for TiO_2 support, fresh and aged Pd/TiO_2 and $Pd\text{-}SiO_2/TiO_2$ catalysts.

significant impact on TiO_2 crystal structure after the loading of Pd and $Pd\text{-}SiO_2$. After hydrothermal aging, the TiO_2 crystallite size increased on both Pd/TiO_2 and $Pd\text{-}SiO_2/TiO_2$ catalysts. However, comparing to Pd/TiO_2-Aged with TiO_2 crystallite size increased from 19.8 to 26.9 nm, $Pd\text{-}SiO_2/TiO_2$-Aged showed a slightly lower degree of crystallite increase from 19.4 to 25.9 nm, suggesting that the colloidal SiO_2 modification suppressed the TiO_2 sintering to a certain extent during hydrothermal aging.

Fig. 3 shows the N_2 adsorption-desorption isotherms and pore-size distributions of all catalysts, and their textural parameters are listed in Table 1. It can be clearly seen that all catalysts showed a type II nitrogen

Table 1
Average crystallite sizes (D_{TiO2}), specific surface areas (S_{BET}), pore volumes, and average pore widths of all catalysts.

Sample	D_{TiO2}[a] (nm)	S_{BET}[b] (m^2/g)	Pore volume[c] (cm^3/g)	Average pore width[c] (nm)
TiO_2	19.3	93	0.26	7.4
Pd/TiO_2	19.8	82	0.27	8.5
Pd/TiO_2-Aged	26.9	49	0.23	15.2
$Pd\text{-}SiO_2/TiO_2$	19.4	87	0.25	7.6
$Pd\text{-}SiO_2/TiO_2$-Aged	25.9	67	0.23	11.2

[a] Calculated according to the Scherrer equation using the FWHM of the (101) plane of TiO_2.
[b] Calculated using multiple-point Brunauer-Emmett-Teller (BET) method.
[c] Determined using non-local density functional theory (DFT) method.

adsorption-desorption isotherm with a type H3 hysteresis loop in the relative pressure (p/p_0) range of 0.7–1.0 (Fig. 3A) [27]. The H3 hysteresis loop could be assignable to the capillary condensation taking place in mesopores, indicates that textural mesopores existed within all samples, [28] as confirmed by the pore-size distributions in Fig. 3B. For fresh Pd/TiO_2 and $Pd\text{-}SiO_2/TiO_2$ catalysts, their specific surface areas (82 and 87 m^2/g, respectively), pore volumes (0.27 and 0.25 cm^3/g, respectively) and the average pore widths (8.5 and 7.6 nm, respectively) were quite similar to those of the pristine TiO_2 support, suggesting that there was no significant contribution from colloidal SiO_2 and Pd to the textural properties of fresh catalysts. After hydrothermal aging, as expected, the specific surface areas and pore volumes greatly decreased and the average pore widths largely increased on Pd/TiO_2-Aged and $Pd\text{-}SiO_2/TiO_2$-Aged catalysts due to the collapse of the small mesoporous structures. However, much lower degree of textural deterioration was observed on $Pd\text{-}SiO_2/TiO_2$-Aged than on Pd/TiO_2-Aged (*e.g.*, 67 *vs.* 49 m^2/g for specific surface areas, and 11.2 *vs.* 15.2 nm for average pore widths), indicating again that the SiO_2 modification showed benefits on stabilizing the structure of Pd/TiO_2 catalyst. It should be noted that, with the collapse of smaller pore structures after hydrothermal aging (Fig. 3B), the average pore widths for Pd/TiO_2-Aged and $Pd\text{-}SiO_2/TiO_2$-Aged catalysts both increased to a certain extent.

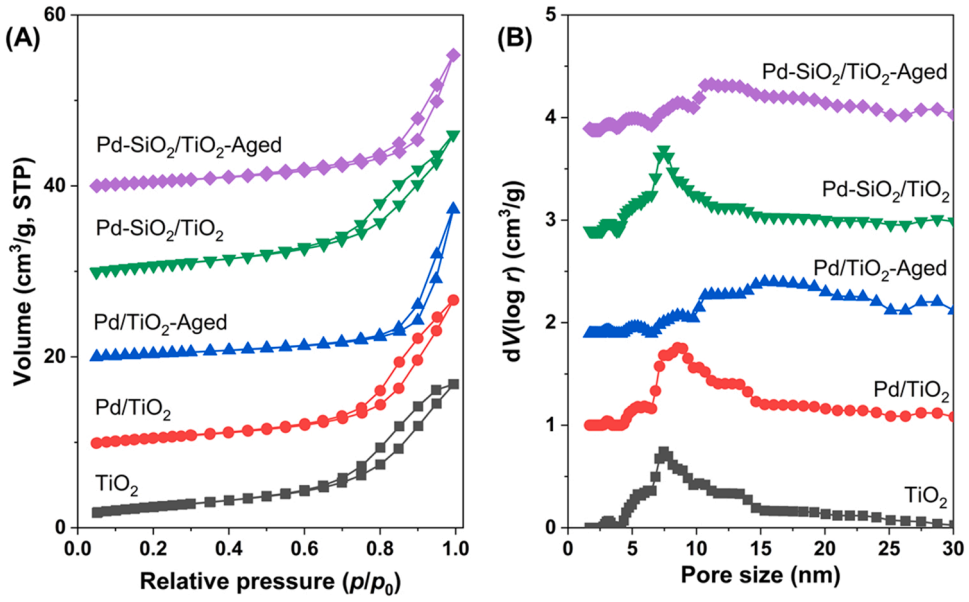

Fig. 3. (A) N_2 adsorption-desorption isotherms and (B) pore-size distributions of TiO_2 support, fresh and aged Pd/TiO_2 and $Pd\text{-}SiO_2/TiO_2$ catalysts.

To confirm the Pd dispersion state and potential interaction between Pd and SiO_2 species, HAADF-STEM and EDS mapping images for both fresh and aged catalysts were collected. As the results shown in Fig. 4 and S2, more highly dispersed Pd nanoparticles with much smaller Pd particle size were present in $Pd\text{-}SiO_2/TiO_2$ catalyst than in Pd/TiO_2 reference catalyst before (5.4 nm *vs.* 9.4 nm) and after (11.4 nm *vs.* 16.6 nm) hydrothermal aging (Figs. S2I, S2S, 4I and 4S). These results clearly suggest the significant positive effect of SiO_2 addition in improving the Pd dispersion and stabilizing Pd species. Although no apparent tracking between Pd and Si was observed on fresh $Pd\text{-}SiO_2/TiO_2$ catalyst (Figs. S2N-S2R), interestingly, obvious tracking between Pd and Si species were present on $Pd\text{-}SiO_2/TiO_2$-Aged catalyst (Fig. 4**N-4R**). Therefore, it can be deduced that hydrothermal aging promoted the formation of abundant $Pd\text{-}SiO_2$ interfaces within $Pd\text{-}SiO_2/TiO_2$-Aged catalyst, which should be highly beneficial for the H_2-SCR reaction.

The oxidation state and local coordination environment of Pd species on all catalysts could be determined by the Pd K-edge XAS results (Fig. 5 and Fig. S3). As shown in Fig. 5A, the Pd K-edge XANES patterns of fresh and aged Pd/TiO_2 and $Pd\text{-}SiO_2/TiO_2$ catalysts were very similar to that of PdO, suggesting the ionic state of Pd species in these catalysts. Fourier transformed EXAFS in R space and EXAFS oscillations in *k* space with curve fitted results for both Pd/TiO_2 and $Pd\text{-}SiO_2/TiO_2$ catalysts before and after aging are shown in Fig. 5B, S3A and Fig. S3B, respectively. Similar to PdO, Pd/TiO_2 and $Pd\text{-}SiO_2/TiO_2$ catalysts only showed Pd-O and Pd-O-Pd bonds, with no Pd-Pd metallic bond observed. As the EXAFS curve fitting parameters shown in Table S2, the coordination numbers (CN) of Pd-O-Pd_1 and Pd-O-Pd_2 shells with different bond lengths in fresh $Pd\text{-}SiO_2/TiO_2$ catalyst were *ca.* 3.0 and 5.4, respectively, of which the latter was lower than that in fresh Pd/TiO_2 catalyst (*ca.* 3.1 and 6.3, respectively). After hydrothermal aging, the CN of Pd-O-Pd_1 and Pd-O-Pd_2 bonds in $Pd\text{-}SiO_2/TiO_2$-Aged catalyst increased to *ca.* 3.4 and 6.8, respectively, but were still slightly lower than that in Pd/TiO_2-Aged catalyst (*ca.* 3.5 and 7.0, respectively). These results suggest the presence of smaller PdO nanoparticles in $Pd\text{-}SiO_2/TiO_2$ and $Pd\text{-}SiO_2/TiO_2$-Aged catalysts comparing to their Pd/TiO_2 and Pd/TiO_2-Aged counterpart catalysts, respectively, which was in consistence with above-mentioned STEM results.

The oxidation state of Pd species in all catalysts was further determined by the XPS technique. As the Pd 3d XPS results shown in Fig. 6A, only Pd^{2+} species were present in all catalysts based on the binding energy (BE) value between 336.5 and 336.8 eV for Pd $3d_{5/2}$ [24,29–31]. The addition of SiO_2 obviously promoted the Pd dispersion and facilitated the Pd species with relatively lower oxidation states, since more intense peak and lower binding energy were observed on $Pd\text{-}SiO_2/TiO_2$ (at 336.5 eV for Pd $3d_{5/2}$) than on Pd/TiO_2 (at 336.8 eV for Pd $3d_{5/2}$). For each catalyst, no apparent change on Pd oxidation state was observed after hydrothermal aging, and $Pd\text{-}SiO_2/TiO_2$ catalyst always showed much higher Pd surface concentration than Pd/TiO_2 before and after aging. As confirmed by H_2-TPR results (Fig. 7, which will be discussed in detail later), the Pd^{2+} species could be easily reduced to Pd^0 below 50 °C by H_2. Therefore, under typical H_2-SCR condition, the Pd species within Pd/TiO_2 and $Pd\text{-}SiO_2/TiO_2$ catalysts were probably in Pd^0 phase. It was reported that the surface Pd^0 species was more active than Pd^{2+} species in the H_2-SCR reaction over Pd-based catalysts [12,19]. The higher surface concentration of Pd^0 species on $Pd\text{-}SiO_2/TiO_2$ catalyst than on Pd/TiO_2 under reaction condition probably contributed to the higher H_2-SCR activity on the former catalyst. As shown in Fig. 6B, the asymmetrical O 1s XPS for each catalyst could be deconvoluted into three components, with the surface lattice oxygen (O_{latt}) species at BE = 529.9–530.0 eV, the surface adsorbed oxygen species ($O_{ads\ I}$) at BE = 531.0–531.3 eV and the surface adsorbed OH species ($O_{ads\ II}$) at BE = 532.6–533.0 eV on oxygen vacancies [32,33]. As the inserted values shown in Fig. 6B, much higher concentration of surface adsorbed oxygen species (O_{ads}/O_{latt} molar ratios, with $O_{ads} = O_{ads\ I} + O_{ads\ II}$) was present on $Pd\text{-}SiO_2/TiO_2$ catalyst than on Pd/TiO_2 catalyst not only before (*i.e.*, 0.84 *vs.* 0.41) but also after (*i.e.*, 0.66 *vs.* 0.15) hydrothermal aging, suggesting that the colloidal SiO_2 addition significantly promoted the formation of oxygen vacancies on $Pd\text{-}SiO_2/TiO_2$ catalyst. Due to the sintering of TiO_2 support under hydrothermal aging condition, the absolute amount of surface adsorbed oxygen species showed some decrease on both aged catalysts, however, much slighter decrease was observed on $Pd\text{-}SiO_2/TiO_2$ confirming again the great benefit from colloidal SiO_2 promoter.

Cryogenic H_2-TPR experiments were carried out to investigate the reducibility of TiO_2 support, fresh and aged Pd/TiO_2 and $Pd\text{-}SiO_2/TiO_2$ catalysts, and the results are illustrated in Fig. 7. For pristine TiO_2, only one reduction peak centered at *ca.* 568 °C corresponding to the reduction of surface Ti^{4+} species was observed [34,35]. After loading with Pd or $Pd\text{-}SiO_2$, the reduction of surface Ti^{4+} species shifted to lower temperatures (*i.e.*, *ca.* 296 °C for Pd/TiO_2 and *ca.* 314 °C for $Pd\text{-}SiO_2/TiO_2$) due to the metal-support interaction between Pd and TiO_2 and the H_2 spillover effect induced by Pd [35–37]. Comparing to Pd/TiO_2 catalyst,

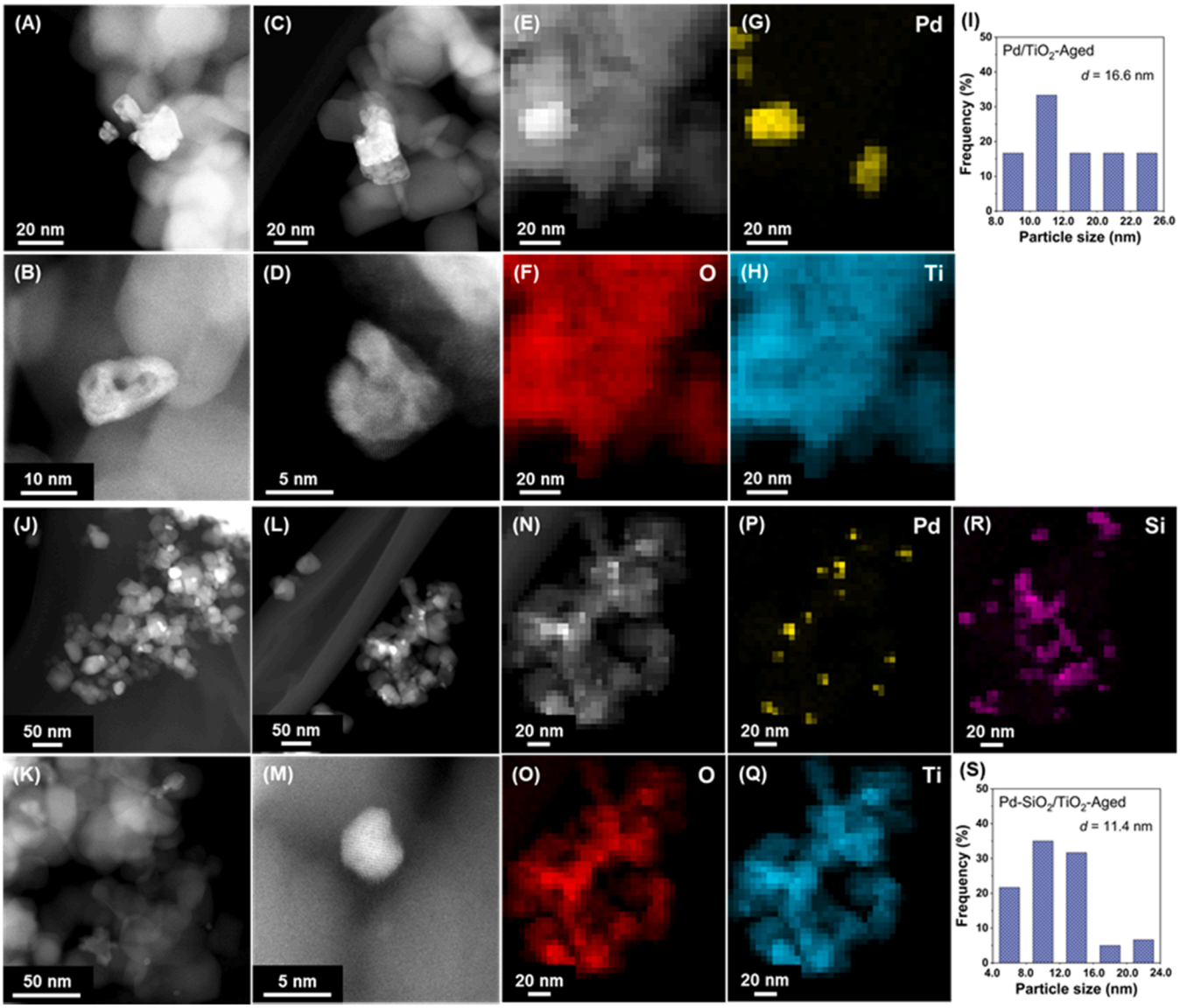

Fig. 4. (A–D, J–M) HAADF-STEM, (E-H, N-R) EDS mapping images and (I, S) Pd particle size distributions for Pd/TiO_2-Aged (A–I) and $Pd\text{-}SiO_2/TiO_2$-Aged (J–S) catalysts.

$Pd\text{-}SiO_2/TiO_2$ catalyst showed higher reduction temperature for surface Ti^{4+} species, indicating that a relatively weaker interaction between Pd and TiO_2 was present in $Pd\text{-}SiO_2/TiO_2$ than in the former. By quantitatively analyzing the reduction peaks in detail, the H_2 consumptions of the samples could be obtained and summarized in Table S3. If the Pd species within the samples were all in PdO phase, the theoretical H_2 consumption should be 94.0 μmol/g. However, the H_2 consumptions of the samples below 50 °C were calculated as 258.5–495.2 μmol/g, which were 2.7–5.3 times of the theoretical H_2 consumption for PdO. Clearly, the species reduced below 50 °C included not only PdO species but also interfacial TiO_2 species. It is interesting that the reduction peak for PdO and interfacial TiO_2 species was observed on fresh $Pd\text{-}SiO_2/TiO_2$ at *ca.* −20 °C, [31,38] which was probably present on fresh Pd/TiO_2 at temperature below −50 °C (thus not captured herein), suggesting a higher Pd dispersion on $Pd\text{-}SiO_2/TiO_2$. After hydrothermal aging, the reduction peak for surface Ti^{4+} species disappeared on both Pd/TiO_2-Aged and $Pd\text{-}SiO_2/TiO_2$-Aged catalysts probably due to the significant decline of TiO_2 surface area. Comparing to the H_2 reduction peak for PdO and interfacial TiO_2 species in Pd/TiO_2-Aged catalyst at *ca.* −18 °C, the reduction peak at lower temperature (*ca.* −26 °C) for species in $Pd\text{-}SiO_2/TiO_2$-Aged catalyst was observed probably due to the formation of abundant $Pd\text{-}SiO_2$ interfaces benefitting the H_2 activation.

To determine the effects of SiO_2 addition on surface acidity and NO adsorption capacity of Pd/TiO_2 catalyst, NH_3-TPD and NO-TPD were performed on TiO_2 support, fresh and aged Pd/TiO_2 and $Pd\text{-}SiO_2/TiO_2$ catalysts. As depicted in Fig. 8A, three NH_3 desorption peaks centered at *ca.* 148 °C, *ca.* 275–310 °C and *ca.* 373 °C were observed on all samples, which could be assigned to the continuous desorption of NH_3 adsorbed on Brønsted acid sites, weak and strong Lewis acid sites, respectively [39,40]. Comparing to the situation on pristine TiO_2 support, much lower NH_3 desorption amount was observed on Pd/TiO_2 and $Pd\text{-}SiO_2/TiO_2$ catalysts due to their lowered surface areas. After aging, the acid sites were further decreased on both Pd/TiO_2 and $Pd\text{-}SiO_2/TiO_2$ catalysts. However, as expected, more acid sites were observed on $Pd\text{-}SiO_2/TiO_2$ than on Pd/TiO_2 before and after hydrothermal aging, suggesting that the SiO_2 addition could enhance the surface acidity to a certain extent.

The catalytic performance is normally linked to the adsorption of reactants on a particular catalyst. Therefore, NO-TPD was performed to determine the NO adsorption-desorption ability on the TiO_2 support and

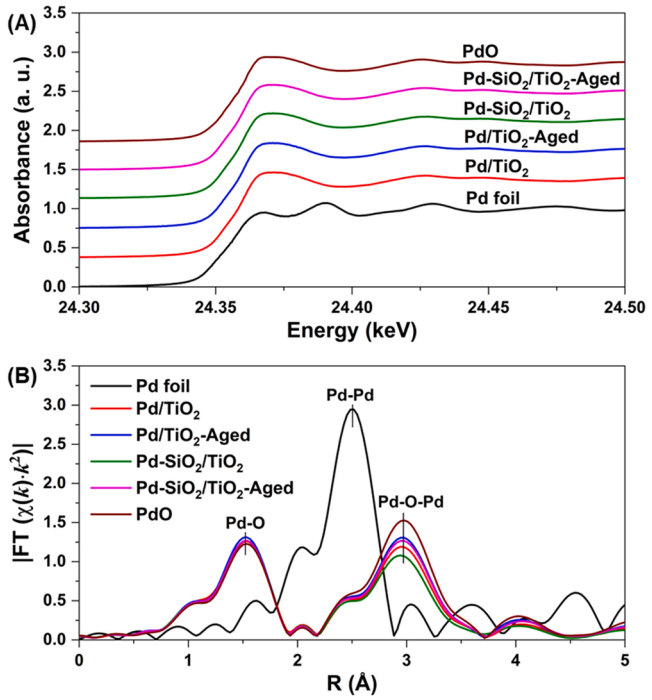

Fig. 5. (A) Normalized XANES and (B) Fourier transformed k^2-weighted EXAFS oscillations in R space for Pd K-edge in fresh and aged Pd/TiO_2 and $Pd\text{-}SiO_2/TiO_2$ catalysts using Pd foil and PdO as references.

Pd catalysts in this work, and the results are shown in Fig. 8B. It can be seen that one broad NO desorption peak centered at *ca.* 355 °C was present on TiO_2 [38,41]. With Pd or $Pd\text{-}SiO_2$ loading, a new and sharp peak for NO desorption probably from Pd sites centered at *ca.* 250 °C was observed in addition to the broad NO desorption from TiO_2. Moreover, the NO desorption peaks on Pd/TiO_2 and $Pd\text{-}SiO_2/TiO_2$ shifted to lower temperatures comparing to that on pristine TiO_2 support, indicating that the $Pd\text{-}TiO_2$ interfaces could benefit the mobility of NO adsorbed species on TiO_2. After aging, the peaks for NO desorption from Pd sites further shifted to much lower temperatures on Pd/TiO_2--Aged (*ca.* 193 °C) and $Pd\text{-}SiO_2/TiO_2$-Aged (*ca.* 187 °C) catalysts, with more intense NO desorption from Pd sites observed on the former. Considering that the Pd particle sizes on fresh catalysts were much smaller than that on aged catalysts, the NO-TPD results clearly suggest that the NO adsorption on smaller Pd particles was much stronger and the NO desorption on larger Pd particles was much easier. Comparing to the situation on Pd/TiO_2-Aged, less NO adsorption and easier NO desorption on $Pd\text{-}SiO_2/TiO_2$-Aged were observed, indicating that the SiO_2 promoter inhibited and weakened the NO adsorption on Pd particles within $Pd\text{-}SiO_2/TiO_2$-Aged catalyst. These results suggested that the improved H_2-SCR activity by SiO_2 addition could be due to the enhanced H_2 activation on $Pd\text{-}SiO_2/TiO_2$-Aged other than the improved NO adsorption.

3.3. Mechanism study of H_2-SCR on Pd/TiO_2-Aged and $Pd\text{-}SiO_2/TiO_2$-Aged catalysts

To further reveal the promotion effect of SiO_2 on the catalytic

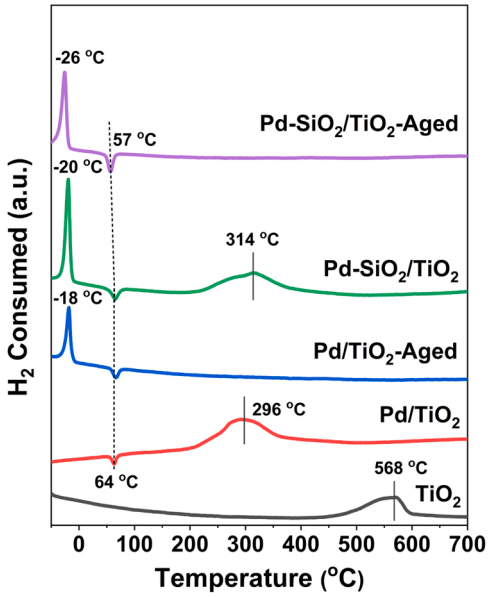

Fig. 7. H_2-TPR profiles for TiO_2 support, fresh and aged Pd/TiO_2 and $Pd\text{-}SiO_2/TiO_2$ catalysts.

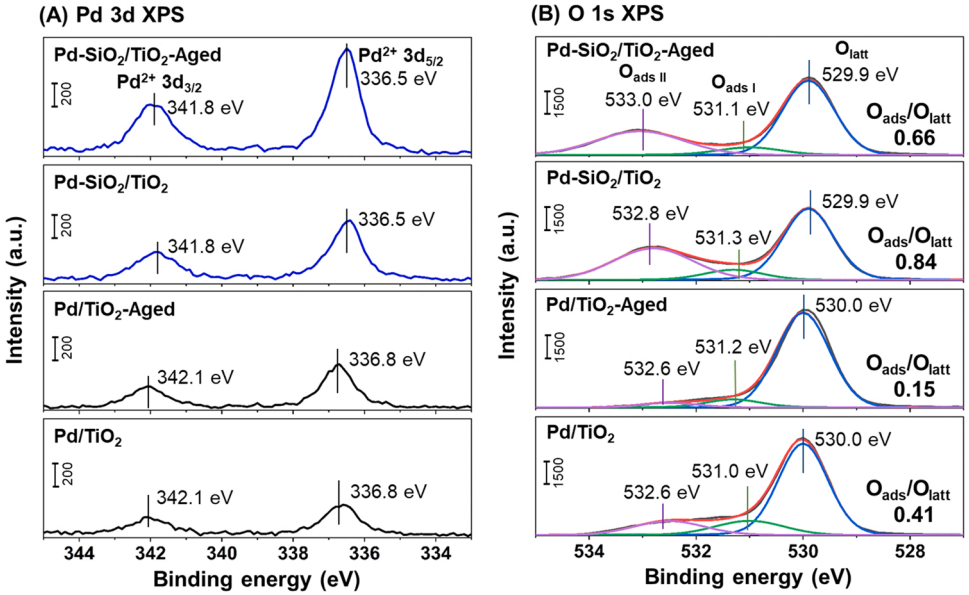

Fig. 6. (A) Pd 3d and (B) O 1s XPS for fresh and aged Pd/TiO_2 and $Pd\text{-}SiO_2/TiO_2$ catalysts.

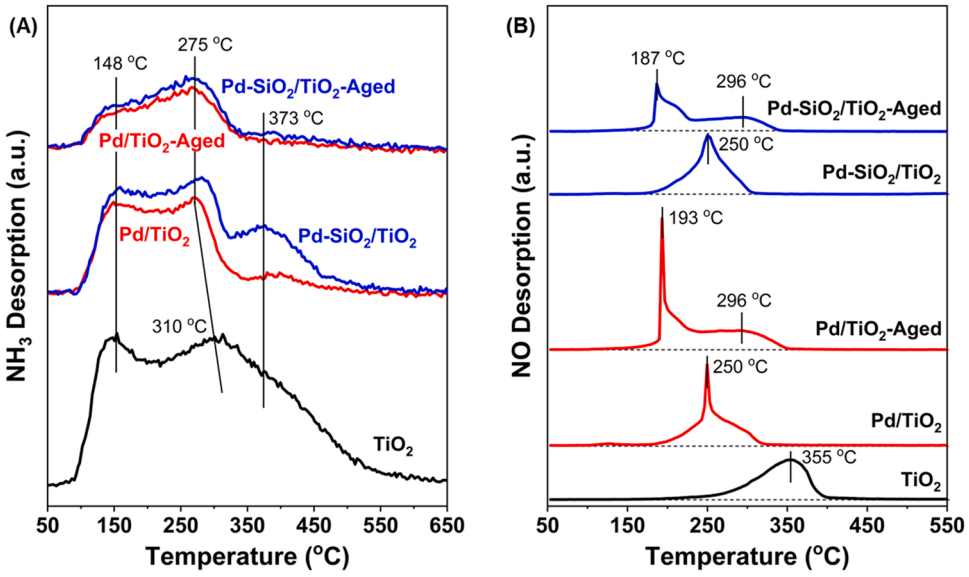

Fig. 8. (A) NH_3-TPD and (B) NO-TPD profiles on TiO_2 support, fresh and aged Pd/TiO_2 and $Pd\text{-}SiO_2/TiO_2$ catalysts.

performance of Pt/TiO_2 catalyst, as shown in Fig. 9, the reaction orders of NO, O_2, H_2 and H_2O in the H_2-SCR reaction were measured. It was observed that the reaction orders showed two distinct ranges of dependency on reactant or H_2O concentration, suggesting that H_2-SCR performance was sensitive to the reaction flow. In details, on Pd/TiO_2-Aged and $Pd\text{-}SiO_2/TiO_2$-Aged catalysts, the NO reaction orders were

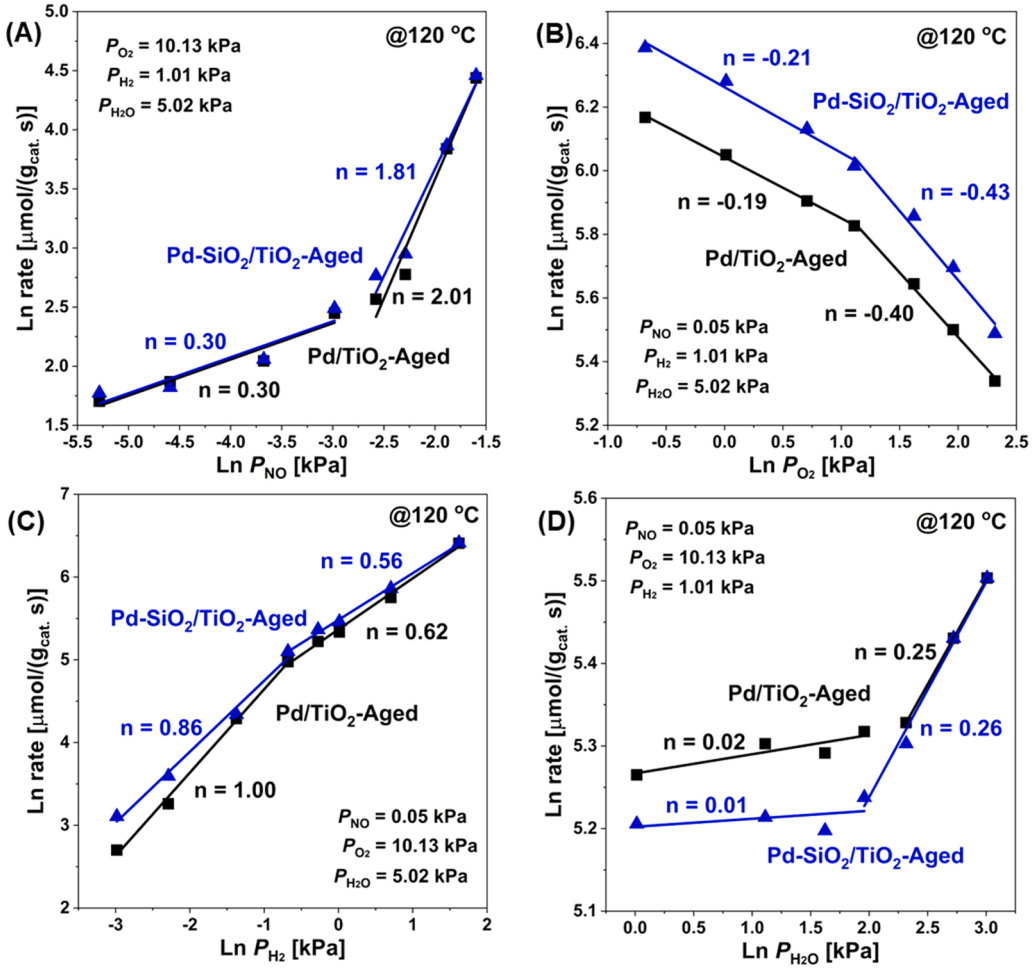

Fig. 9. Kinetics study for the determination of (A) NO, (B) O_2, (C) H_2, and (D) H_2O reaction orders in H_2-SCR of NO on Pd/TiO_2-Aged and $Pd\text{-}SiO_2/TiO_2$-Aged catalysts.

determined as 0.30 and 0.30, respectively, when the NO concentration was below 500 ppm, or 2.01 and 1.81, respectively, when the NO concentration was above 500 ppm (Fig. 9A); the O_2 reaction orders were determined as −0.19 and −0.21, respectively, when the O_2 concentration was below 3 %, or −0.40 and −0.43, respectively, when the O_2 concentration was above 3 % (Fig. 9B); the H_2 reaction orders were determined as 1.00 and 0.86, respectively, when the H_2 concentration was below 0.5 %, or 0.62 and 0.56, respectively, when the H_2 concentration was above 0.5 % (Fig. 9C); the H_2O reaction orders were 0.02 and 0.01 (approximated to 0), respectively, when the H_2O concentration was below 7 %, or 0.25 and 0.26, respectively, when the H_2O concentration was above 7 % (Fig. 9D). Therefore, under the activity testing conditions in this work (*i.e.*, 500 ppm NO, 1 % H_2, 10 % O_2, 5 % CO_2 and 5 % H_2O), the H_2-SCR reaction rates on Pd/TiO_2-Aged and Pd-SiO_2/TiO_2-Aged could be expressed as $r(\text{Pd/TiO}_2\text{-Aged}) = k_1 \cdot [NO]^{0.30} \cdot [H_2]^{0.62} \cdot [O_2]^{-0.40}$ and $r(\text{Pd-SiO}_2\text{/TiO}_2\text{-Aged}) = k_2 \cdot [NO]^{0.30} \cdot [H_2]^{0.56} \cdot [O_2]^{-0.43}$, respectively (with k_1 and k_2 as constants). It is noteworthy that the NO and H_2 reaction orders on both Pd/TiO_2-Aged (0.30 and 0.62) and Pd-SiO_2/TiO_2-Aged (0.30 and 0.56) were much lower than 1, which can be explained by the fact that the H_2-SCR reaction on both catalysts involved adsorbed NO (*i.e.*, surface-adsorbed nitrate species) and adsorbed H_2 (*i.e.*, dissociated H* species), following the Langmuir-Hinshelwood (L-H) mechanism. Except the lower H_2 reaction order measured on Pd-SiO_2/TiO_2-Aged (0.56) than on Pd/TiO_2-Aged (0.62), the NO, O_2, H_2O reaction orders in H_2-SCR reaction on both catalysts were rather close. These results suggest that the SiO_2 promoter in Pd-SiO_2/TiO_2-Aged catalyst played a critical role in the H_2 adsorption and activation, which in turn benefited the NO reduction efficiency. It should be noted that negative O_2 reaction orders were observed on both catalysts due to the possible consumption of H_2 by O_2 or the competitive adsorption between O_2 and NO at Pd-TiO_2 interfaces, with the latter one as the most probable reason. The higher O_2 concentration, the lower NO adsorption and thus the lower H_2-SCR activity achieved on both catalysts.

To further study the effects of H_2O and O_2 on the H_2-SCR activity, the catalysts were also evaluated under the testing conditions with/without H_2O (Fig. 10A and S4A) and with/without O_2 in the dry reaction flow (Fig. 10B and S4B). It can be observed from Fig. 10A that H_2O showed negative impact on the H_2-SCR activity over both Pd/TiO_2-Aged and Pd-SiO_2/TiO_2-Aged catalysts, particularly at high temperatures. Comparing to the more severe deactivation on Pd/TiO_2-Aged catalyst with significant decline of NO_x conversion and N_2 selectivity (*i.e.*, increase of N_2O yield) in the presence of H_2O (Fig. 10A and S4A), much slighter decrease of NO_x conversion and even a slight increase of N_2 selectivity (*i.e.*, decline of N_2O yield) were observed on Pd-SiO_2/TiO_2-Aged catalyst. Such results suggest that the SiO_2 addition showed obvious promotion effect on improving the H_2O resistance of Pd-SiO_2/TiO_2-Aged catalyst. It should be noted that the Pd-SiO_2/TiO_2-Aged catalyst constantly outperformed the Pd/TiO_2-Aged catalyst in the H_2-SCR reaction under conditions with/without H_2O. As illustrated in Fig. 10B and S4B, with the removal of O_2 from the H_2-SCR reaction flow, the NO_x reduction performance on Pd/TiO_2-Aged and Pd-SiO_2/TiO_2-Aged catalysts could be greatly improved, especially on Pd/TiO_2-Aged. This negative effect of O_2 on NO_x reduction activity was probably mainly due to the competitive adsorption between O_2 and NO, which was in consistence with the results of kinetics study. The much slighter deactivation effect of O_2 observed on Pd-SiO_2/TiO_2-Aged catalyst than on Pd/TiO_2-Aged catalyst indicated that the O_2 tolerance could be remarkably improved through the simple SiO_2 modification.

To study the effect of NO on H_2 oxidation by O_2, the H_2 oxidation testing under dry conditions with/without NO was conducted, and the results are shown in Fig. 10C. It can be clearly observed that Pd-SiO_2/TiO_2-Aged catalyst showed much higher H_2 oxidation activity than Pd/TiO_2-Aged catalyst under NO free condition. Upon NO addition, the H_2 oxidation activity decreased on both catalysts, but Pd-SiO_2/TiO_2-Aged catalyst still exhibited much higher activity than Pd/TiO_2-Aged catalyst. As discussed above, the negative effect of NO on H_2 oxidation activity can also be explained by the competitive adsorption between NO and O_2. The constantly higher H_2 oxidation activity on Pd-SiO_2/TiO_2-Aged catalyst than on Pd/TiO_2-Aged catalyst was associated with the superior H_2 adsorption and activation ability on the former catalyst with abundant Pd-SiO_2 interfaces as verified above.

To determine if the NO oxidation occurred during the H_2-SCR

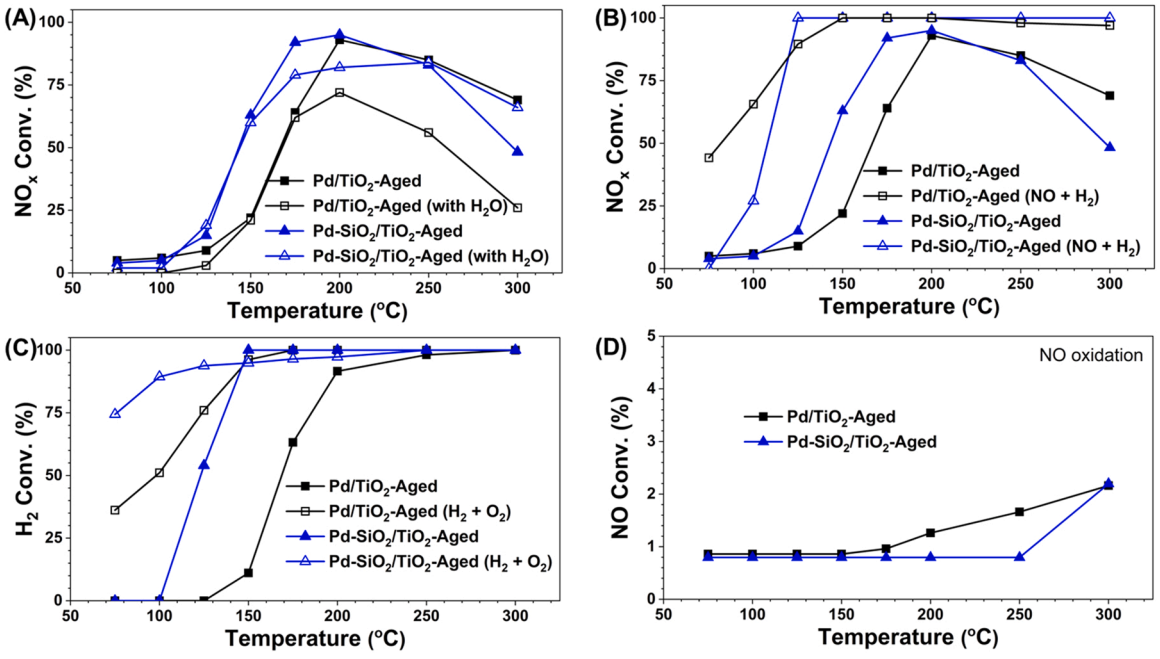

Fig. 10. (A) H_2O effect on the H_2-SCR activity under 500 ppm NO, 1 % H_2, 10 % O_2, 5 % CO_2 + 5 % H_2O (if used); (B) O_2 effect on the NO_x reduction activity by H_2 under 500 ppm NO, 1 % H_2, 10 % O_2 (if used); (C) NO effect on the H_2 oxidation activity by O_2 under 1 % H_2, 10 % O_2, 500 ppm NO (if used); and (D) NO oxidation activity under 500 ppm NO, 10 % O_2, on Pd/TiO_2-Aged and Pd-SiO_2/TiO_2-Aged catalysts. Other reaction conditions: Ar as balance, WHSV = 461,540 mL·g^{-1}·h^{-1} (GHSV = 565,335 h^{-1}).

reaction, the NO oxidation activity on both catalysts was further evaluated. As demonstrated in Fig. 10D, Pd/TiO_2-Aged catalyst showed relatively higher NO oxidation activity than Pd-SiO_2/TiO_2-Aged catalyst due to the presence of larger Pd nanoparticles in the former. It should be noted that ultra-low NO oxidation activity (with NO conversion < 3 %) was observed on both catalysts below 300 °C, indicating that there was no significant NO oxidation on Pd/TiO_2-Aged and Pd-SiO_2/TiO_2-Aged catalysts during the H_2-SCR process.

The surface acidity on both catalysts were determined using *in situ* DRIFTS experiments of NH_3 adsorption and desorption. It was observed that the adsorbed NH_3 species on Lewis acid sites (1170, 1230–1233, 1476–1495, 1593–1594, 3157, 3260, 3349 and 3401 cm^{-1}) and the adsorbed NH_4^+ species on Brønsted acid sites (1436–1439, 1661–1664 cm^{-1}) were present on both Pd/TiO_2-Aged and Pd-SiO_2/TiO_2-Aged catalysts at 50 °C (Figs. 11A and C) [42–44]. Interestingly, on Pd-SiO_2/TiO_2-Aged catalyst, the vibration peaks of H-Si-O bonds (1870 and 1996 cm^{-1}) were also detected due to the adsorption of NH_3 species on SiO_2 sites (Fig. 11C) [45,46]. This result indicates that the SiO_2 addition increased the Lewis acid sites on Pd-SiO_2/TiO_2-Aged catalyst and significantly promoted the NH_3 dissociation. Similar to the observation from NH_3-TPD results (Fig. 8), the temperature-dependent DRIFTS results show that the NH_3 species adsorbed on Lewis acid sites were more stable than the NH_4^+ species adsorbed on Brønsted acid sites on both catalysts (Figs. 11B and D), with the former species being observable even at temperatures up to 250 °C. Furthermore, even at 250 °C, the H-Si-O species could still be observed on Pd-SiO_2/TiO_2-Aged catalyst, suggesting the possible involvement of dissociated H species in the enhanced H_2-SCR process on this modified catalyst.

To further confirm if the H-Si-O species could be present on catalyst surface during H_2-SCR process, the *in situ* DRIFTS were collected on Pd/TiO_2-Aged and Pd-SiO_2/TiO_2-Aged catalysts under H_2-SCR reaction flow at 150 °C (Fig. 12). Upon the introduction of NO + H_2 + O_2 into the DRIFTS cell, the bands for the *in situ* formed OH species at *ca.* 1624 cm^{-1} appeared immediately on both catalysts [46]. The bands assigned to bridging bidentate nitrates at *ca.* 1605 cm^{-1}, chelating bidentate nitrates at *ca.* 1583 cm^{-1}, and monodentate nitrates at 1510 and 1295 cm^{-1} increased gradually, [22,43,47,48] and achieved stable after 10 min. Comparing to the situation on Pd/TiO_2-Aged catalyst, more intense bridging bidentate nitrates was present on Pd-SiO_2/TiO_2-Aged catalyst. Besides, the bands attributed to H-Si-O species could be clearly observed on Pd-SiO_2/TiO_2-Aged catalyst under the H_2-SCR reaction flow, which were absent on the Pd/TiO_2-Aged reference. Different from the H species within H-Si-O resulting from the NH_3 adsorption and dissociation (Fig. 11C and D), under the H_2-SCR reaction flow, the H species herein should come from the dissociated H_2, indicating the promotion effect of SiO_2 addition on H_2 adsorption and dissociation.

To reveal the reactive surface species and mechanism for the H_2-SCR reaction, *in situ* DRIFTS under different reaction flows on Pd/TiO_2-Aged and Pd-SiO_2/TiO_2-Aged catalysts were recorded at 150 °C. As depicted in Fig. 13, under the H_2-SCR reaction flow, besides of the H-Si-O species observed only on Pd-SiO_2/TiO_2-Aged catalyst, adsorbed OH species and nitrates were present on both catalysts as mentioned above. Once changing the H_2-SCR reaction flow (NO + H_2 + O_2) to NO + O_2 flow, the adsorbed OH species (1624 cm^{-1}) and monodentate nitrates (1505 and 1295 cm^{-1}) disappeared, while the bridging bidentate nitrates (1605 cm^{-1}) increased on both catalysts. Since there was no H_2 in the flow, the disappearance of OH species could be explained by the absence of H_2 oxidation reaction. It was reported that H_2 could assist the conversion of nitrites and bidentate nitrates to monodentate and bridging nitrates [49]. The absence of monodentate nitrates under the condition without H_2 could be due to the insufficient conversion of nitrites and bidentate nitrates. Under such condition, it should be noted that the H-Si-O species was also absent on Pd-SiO_2/TiO_2-Aged catalyst, confirming again that the H species within H-Si-O was resulted from the H_2

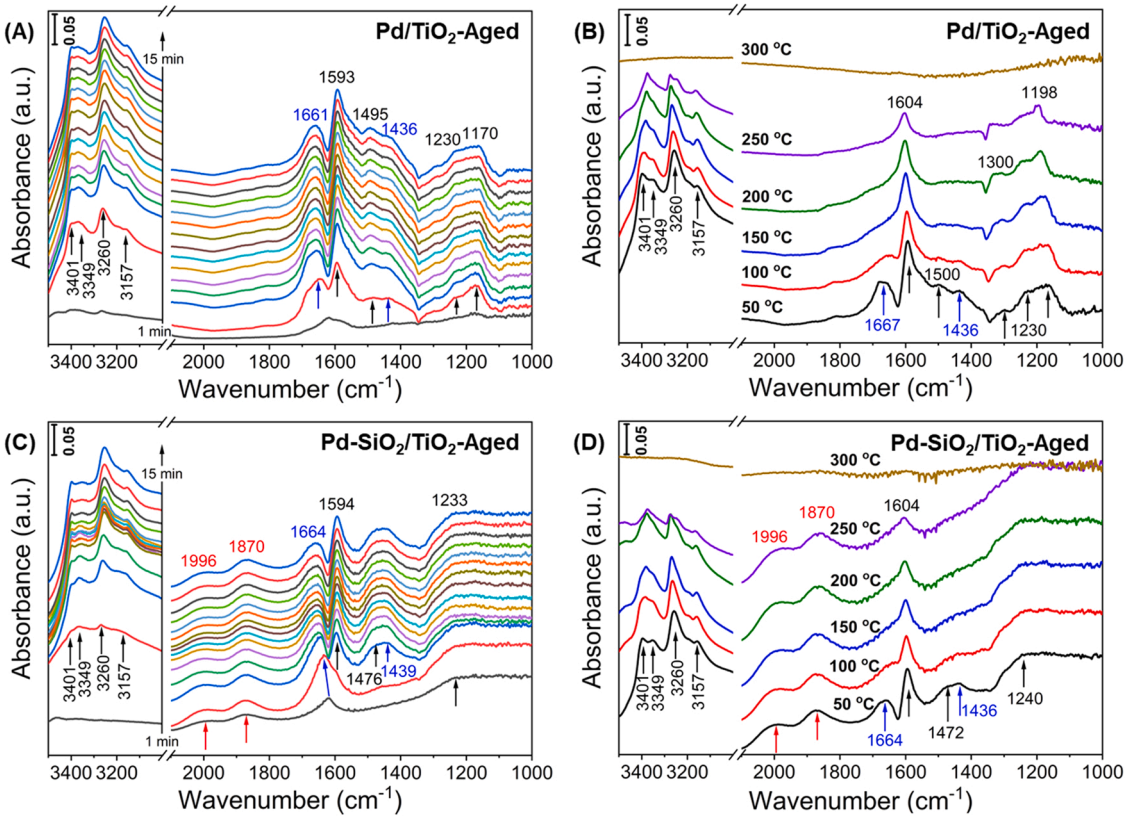

Fig. 11. *In situ* DRIFTS of (A, C) NH_3 adsorption at 50 °C as a function of time and (B, D) NH_3 desorption at different temperatures on (A, B) Pd/TiO_2-Aged and (C, D) Pd-SiO_2/TiO_2-Aged catalysts.

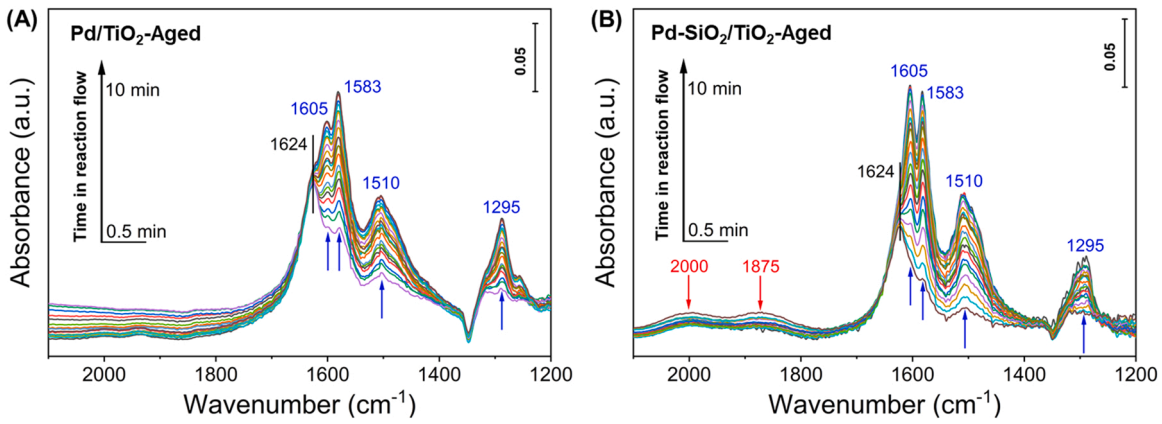

Fig. 12. *In situ* DRIFTS under H_2-SCR reaction flow (500 ppm NO + 1 % H_2 + 10 % O_2) on (A) Pd/TiO_2-Aged and (B) Pd-SiO_2/TiO_2-Aged catalysts at 150 °C.

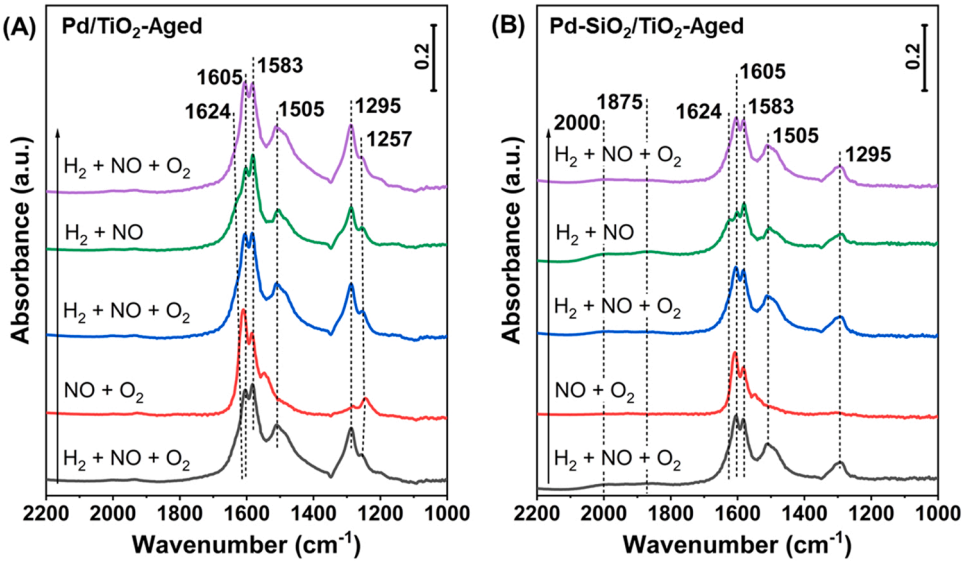

Fig. 13. *In situ* DRIFTS under different reaction flows on (A) Pd/TiO_2-Aged and (B) Pd-SiO_2/TiO_2-Aged catalysts at 150 °C. The spectra shown in the figures were collected under steady-state conditions.

dissociation. After switching back to H_2-SCR reaction flow, the adsorbed OH species, monodentate nitrates and H-Si-O species (only on Pd-SiO_2/TiO_2-Aged catalyst) recovered, and the bridging bidentate nitrates decreased on both catalysts. These results clearly suggest that the adsorbed bridging bidentate nitrates were reactive on the catalyst surface and the monodentate nitrates were significant intermediate species during the H_2-SCR reaction. To further confirm the reactivity of adsorbed bridging bidentate nitrates, the spectra under H_2 + NO flow were also collected. It can be clearly observed that the adsorbed bridging bidentate nitrates showed further decrease in intensity as the H_2-SCR activity increased under O_2-free condition. With the O_2 introduced back to the reaction flow, the adsorbed bridging bidentate nitrates restored the intensity on both catalysts. The above results clearly suggest that the adsorbed bridging bidentate nitrates were the reactive species in the H_2-SCR of NO on Pd/TiO_2-Aged and Pd-SiO_2/TiO_2-Aged catalysts. It is also noteworthy that, under the H_2-SCR condition and other conditions, the band intensity or the surface coverage of nitrate species on Pd-SiO_2/TiO_2-Aged catalyst was constantly lower than that on Pd/TiO_2-Aged catalyst, probably suggesting that the SiO_2 addition could mitigate the over-strong adsorption of nitrates on the catalyst surface or the enhanced H_2 dissociation at Pd-SiO_2 interface (by forming H-Si-O) could help reduce the reactive nitrate species more effectively.

In brief summary, on both Pd/TiO_2-Aged and Pd-SiO_2/TiO_2-Aged catalysts, the H_2-SCR of NO mainly followed the L-H mechanism. As illustrated in Fig. 14, on Pd-SiO_2/TiO_2-Aged catalyst, the adsorbed bridging bidentate nitrates originated from NO adsorption on TiO_2 reacted with the dissociated H* species on Pd sites at the Pd-TiO_2 interfaces, where the monodentate nitrate species as intermediates were formed at the same time. With further reduction by H* species, the monodentate nitrates species could be converted to N_2 and H_2O. Comparing to Pd/TiO_2-Aged catalyst, Pd-SiO_2/TiO_2-Aged catalyst with abundant Pd-SiO_2 interfaces and smaller Pd nanoparticles could facilitated the H_2 adsorption and dissociation, thus accelerating the H_2-SCR

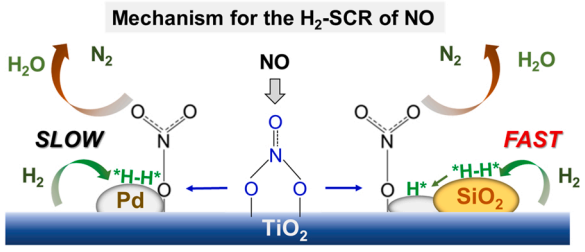

Fig. 14. The mechanism scheme for H_2-SCR of NO on Pd/TiO_2-Aged and Pd-SiO_2/TiO_2-Aged catalysts.

process.

4. Conclusions

In this work, a significant promotion effect of colloidal SiO_2 on Pd/TiO_2 catalyst for the H_2-SCR of NO was reported. With the simple modification by colloidal SiO_2 using co-IWI method with Pd precursor, both the H_2-SCR activity and N_2 selectivity on Pd-SiO_2/TiO_2 catalyst could be greatly enhanced both before and after hydrothermal aging. The highest H_2-SCR activity could be achieved on the Pd-SiO_2/TiO_2 catalyst with an optimal SiO_2 loading of 8 wt%. It was demonstrated that the SiO_2 addition not only increased the Pd dispersion but also benefitted the formation of more oxygen vacancies on Pd-SiO_2/TiO_2 catalyst. With the help from SiO_2 promoter, the active Pd species could be well stabilized on TiO_2 support through the formation of rich Pd-SiO_2 interfaces during the long-term hydrothermal aging process. As verified by the kinetics study and *in situ* DRIFTS experiments, the H_2-SCR of NO on Pd/TiO_2 and Pd-SiO_2/TiO_2 catalysts mainly followed the L-H mechanism, in which the adsorbed bridging bidentate nitrates on TiO_2 could react with dissociated H_2 species on Pd sites. On the promoted Pd-SiO_2/TiO_2 catalyst, the Pd-TiO_2 interfaces could facilitate the NO adsorption and activation, and more importantly the Pd-SiO_2 interfaces could benefit the H_2 adsorption and dissociation forming more reactive H*, thus contributing to its greatly improved H_2-SCR activity. Furthermore, it was verified that the monodentate nitrates were significant intermediate species during the H_2-SCR process on both Pd/TiO_2 and Pd-SiO_2/TiO_2 catalysts.

CRediT authorship contribution statement

Shaohua Xie: Methodology, Investigation, Formal analysis, Visualization, Writing – original draft. **Yuejin Li:** Investigation, Writing – review & editing. **Chunying Wang:** Investigation. **Ke-Bin Low:** Investigation. **Kailong Ye:** Investigation. **Daekun Kim:** Investigation. **Xing Zhang:** Investigation. **Yaobin Li:** Investigation, Resources. **Yan Zhang:** Investigation, Resources. **Fengyuan Shi:** Investigation, Resources. **Lu Ma:** Investigation, Resources. **Steven N. Ehrlich:** Investigation, Resources. **Fudong Liu:** Conceptualization, Methodology, Investigation, Writing – review & editing, Funding acquisition, Supervision, Resources.

Declaration of Competing Interest

The authors declare that they have no known competing financial interests or personal relationships that could have appeared to influence the work reported in this paper.

Data Availability

Data will be made available on request.

Acknowledgements

This work was supported by the research fund from BASF Corporation and the Startup Fund (F. L.) from the University of Central Florida (UCF). S. X., D. K. and X. Z. thank the support from the Preeminent Postdoctoral Program (P3) at UCF. F. L. sincerely thanks Mr. Franck Thibaut and Ms. Corinne Lehaut from Tronox Inc., and Dr. David M. Chapman from W. R. Grace & Co for providing raw materials in catalyst synthesis. This research used beamline 7-BM (QAS) of the National Synchrotron Light Source II, a U.S. Department of Energy (DOE) Office of Science User Facility operated for the DOE Office of Science by Brookhaven National Laboratory under Contract No. DE-SC0012704. This work made use of instruments in the Electron Microscopy Core of UIC's Research Resources Center.

Appendix A. Supporting information

Supplementary data associated with this article can be found in the online version at doi:10.1016/j.apcatb.2023.122437.

References

[1] R. Jeeragal, K.A. Subramanian, Experimental investigation for NO_x emission reduction in hydrogen fueled spark ignition engine using spark timing retardation, exhaust gas recirculation and water injection techniques, J. Therm. Sci. 28 (2019) 789–800.
[2] Z. Liu, J. Li, S.I. Woo, Recent advances in the selective catalytic reduction of NO_x by hydrogen in the presence of oxygen, Energy Environ. Sci. 5 (2012) 8799–8814.
[3] Z. Hu, R.T. Yang, 110th anniversary: recent progress and future challenges in selective catalytic reduction of NO by H_2 in the Presence of O_2, Ind. Eng. Chem. Res. 58 (2019) 10140–10153.
[4] S. Verhelst, P. Maesschalck, N. Rombaut, R. Sierens, Increasing the power output of hydrogen internal combustion engines by means of supercharging and exhaust gas recirculation, Int. J. Hydrogen Energy 34 (2009) 4406–4412.
[5] P. Granger, F. Dhainaut, S. Pietrzik, P. Malfoy, A.S. Mamede, L. Leclercq, G. Leclercq, An overview: comparative kinetic behaviour of Pt, Rh and Pd in the NO + CO and NO + H_2 reactions, Top. Catal. 39 (2006) 65–76.
[6] C.N. Costa, A.M. Efstathiou, Low-temperature H_2-SCR of NO on a novel Pt/MgO-CeO_2 catalyst, Appl. Catal. B: Environ. 72 (2007) 240–252.
[7] C.N. Costa, A.M. Efstathiou, Mechanistic aspects of the H_2-SCR of NO on a Novel Pt/MgO-CeO_2 catalyst, J. Phys. Chem. C 111 (2007) 3010–3020.
[8] Z. Hong, X. Sun, Z. Wang, G. Zhao, X. Li, Z. Zhu, Pt/SSZ-13 as an efficient catalyst for the selective catalytic reduction of NO_x with H_2, Catal. Sci. Technol. 9 (2019) 3994–4001.
[9] M. Komatsubara, A. Koga, M. Tanaka, R. Hagiwara, M. Iwamoto, Three pathways to selective catalytic reduction of NO over Pt/Nb-AlMCM-41 under H_2 with excess O_2, Catal. Sci. Technol. 6 (2016) 7398–7407.
[10] Z. Liu, J. Wu, C. Hardacre, Research progress in the selective catalytic reduction of NO_x by H_2 in the presence of O_2, Catal. Surv. Asia 22 (2018) 146–155.
[11] Y. Zhang, H. Zeng, B. Jia, Z. Liu, Selective catalytic reduction of NO_x by H_2 over a novel Pd/FeTi catalyst, Catal. Today 360 (2021) 213–219.
[12] Y. Zhang, H. Zeng, B. Jia, Z. Wang, Z. Liu, Selective catalytic reduction of NO by H_2 over Pd/TiO_2 catalyst, Chin. J. Catal. 40 (2019) 849–855.
[13] A. Ueda, T. Nakao, M. Azuma, T. Kobayashi, Two conversion maxima at 373 and 573 K in the reduction of nitrogen monoxide with hydrogen over Pd/TiO_2 catalyst, Catal. Today 45 (1998) 135–138.
[14] M. Borchers, K. Keller, P. Lott, O. Deutschmann, Selective catalytic reduction of NO_x with H_2 for cleaning exhausts of hydrogen engines: Impact of H_2O, O_2, and NO/H_2 ratio, Ind. Eng. Chem. Res. 60 (2021) 6613–6626.
[15] Z. Savva, K.C. Petallidou, C.M. Damaskinos, G.G. Olympiou, V.N. Stathopoulos, A. M. Efstathiou, H_2-SCR of NO_x on low-SSA CeO_2-supported Pd: the effect of Pd particle size, Appl. Catal. A: Gen. 615 (2021), 118062.
[16] V.K. Patel, S. Sharma, Effect of oxide supports on palladium based catalysts for NO reduction by H_2-SCR, Catal. Today 375 (2021) 591–600.
[17] Q. Yu, F. Kong, L. Li, G. Wu, N. Guan, Fast catalytic reduction of NO_x by H_2 over Pd-based catalysts, Chin. J. Catal. 31 (2010) 261–263.
[18] Z. Liu, Y. Lu, L. Yuan, L. Ma, L. Zheng, J. Zhang, T. Hu, Selective catalytic reduction of NO_x with H_2 over WO_3 promoted Pt/TiO_2 catalyst, Appl. Catal. B: Environ. 188 (2016) 189–197.
[19] J. Li, G. Wu, N. Guan, L. Li, NO selective reduction by hydrogen over bimetallic Pd-Ir/TiO_2 catalyst, Catal. Commun. 24 (2012) 38–43.
[20] K. Duan, Z. Liu, J. Li, L. Yuan, H. Hu, S.I. Woo, Novel Pd-Au/TiO_2 catalyst for the selective catalytic reduction of NO_x by H_2, Catal. Commun. 57 (2014) 19–22.
[21] Z. Hu, T. Zhang, D. Li, R.T. Yang, Understanding the promotional effect of 3d transition metals (Fe, Co, Cu) on Pd/TiO_2 for H_2-SCR, Catal. Sci. Technol. 11 (2021) 886–894.
[22] Z. Hu, X. Yong, D. Li, R.T. Yang, Synergism between palladium and nickel on Pd-Ni/TiO_2 for H_2-SCR: a transient DRIFTS study, J. Catal. 381 (2020) 204–214.
[23] K. Duan, Z. Liu, L. Yuan, Selective catalytic reduction of NO_x by hydrogen over modified Pd/TiO_2-Al_2O_3 catalyst under lean-burn conditions, Sci. Bull. 59 (2014) 3973–3979.
[24] K. Duan, B. Chen, T. Zhu, Z. Liu, Mn promoted Pd/TiO_2-Al_2O_3 catalyst for the selective catalytic reduction of NO by H_2, Appl. Catal. B: Environ. 176–177 (2015) 618–626.
[25] K. Duan, Z. Wang, C. Hardacre, Z. Liu, S. Chansai, C. Stere, Promoting effect of Au on Pd/TiO_2 catalyst for the selective catalytic reduction of NO_x by H_2, Catal. Today 332 (2019) 69–75.
[26] G.C. Mondragón Rodríguez, B. Saruhan, Effect of Fe/Co-ratio on the phase composition of Pd-integrated perovskites and its H_2-SCR of NO_x performance, Appl. Catal. B: Environ. 93 (2010) 304–313.
[27] M. Thommes, Physical adsorption characterization of nanoporous materials, Chem. Ing. Tech. 82 (2010) 1059–1073.
[28] M. Thommes, K. Kaneko, A.V. Neimark, J.P. Olivier, F. Rodriguez-Reinoso, J. Rouquerol, K.S.W. Sing, Physisorption of gases, with special reference to the evaluation of surface area and pore size distribution (IUPAC Technical Report), Pure Appl. Chem. 87 (2015) 1051–1069.
[29] E.M. Slavinskaya, R.V. Gulyaev, A.V. Zadesenets, O.A. Stonkus, V.I. Zaikovskii, Y. V. Shubin, S.V. Korenev, A.I. Boronin, Low-temperature CO oxidation by Pd/CeO_2

catalysts synthesized using the coprecipitation method, Appl. Catal. B: Environ. 166–167 (2015) 91–103.
[30] S. Xie, Z. Wang, W. Tan, Y. Zhu, S. Collier, L. Ma, S.N. Ehrlich, P. Xu, Y. Yan, T. Xu, J. Deng, F. Liu, Highly active and stable palladium catalysts on novel ceria-alumina supports for efficient oxidation of carbon monoxide and hydrocarbons, Environ. Sci. Technol. 55 (2021) 7624–7633.
[31] C. Wang, Y. Li, C. Zhang, X. Chen, C. Liu, W. Weng, W. Shan, H. He, A simple strategy to improve Pd dispersion and enhance Pd/TiO_2 catalytic activity for formaldehyde oxidation: The roles of surface defects, Appl. Catal. B: Environ. 282 (2021).
[32] Y. Liu, H. Dai, Y. Du, J. Deng, L. Zhang, Z. Zhao, Lysine-aided PMMA-templating preparation and high performance of three-dimensionally ordered macroporous $LaMnO_3$ with mesoporous walls for the catalytic combustion of toluene, Appl. Catal. B: Environ. 119–120 (2012) 20–31.
[33] H. Arandiyan, H. Dai, J. Deng, Y. Liu, B. Bai, Y. Wang, X. Li, S. Xie, J. Li, Three-dimensionally ordered macroporous $La_{0.6}Sr_{0.4}MnO_3$ with high surface areas: Active catalysts for the combustion of methane, J. Catal. 307 (2013) 327–339.
[34] S. Luo, L. Barrio, T.-D. Nguyen-Phan, D. Vovchok, A.C. Johnston-Peck, W. Xu, E. A. Stach, J.A. Rodriguez, S.D. Senanayake, Importance of low dimensional CeO_x nanostructures in Pt/CeO_x-TiO_2 catalysts for the water-gas shift reaction, J. Phys. Chem. C 121 (2017) 6635–6642.
[35] B. Tapin, F. Epron, C. Especel, B.K. Ly, C. Pinel, M. Besson, Study of monometallic Pd/TiO_2 catalysts for the hydrogenation of succinic acid in aqueous phase, ACS Catal. 3 (2013) 2327–2335.
[36] N.S. Babu, N. Lingaiah, N. Pasha, J.V. Kumar, P.S.S. Prasad, Influence of particle size and nature of Pd species on the hydrodechlorination of chloroaromatics: Studies on Pd/TiO_2 catalysts in chlorobenzene conversion, Catal. Today 141 (2009) 120–124.
[37] C. Li, K. Sivaranjani, J.M. Kim, Synthesis of alkali promoted mesoporous, nanocrystalline Pd/TiO_2 catalyst for water gas shift reaction, Catal. Today 265 (2016) 45–51.
[38] J. Watson, Adsorption characteristics of sol-gel Gd-Pd/TiO_2 catalysts in reduction of nitric oxide with CH_4: DRIFTS and TPD, J. Catal. 210 (2002) 295–312.
[39] M.E. Manríquez, T. López, R. Gómez, J. Navarrete, Preparation of TiO_2-ZrO_2 mixed oxides with controlled acid-basic properties, J. Mol. Catal. A 220 (2004) 229–237.
[40] G. Žerjav, A. Pintar, M. Ferentz, M. Landau, A. Haimovich, A. Goldbourt, M. Herskowitz, Effect of surface chemistry and crystallographic parameters of TiO_2 anatase nanocrystals on photocatalytic degradation of bisphenol A, Catalysts 9 (2019) 447.
[41] Y. Wang, T. Shi, Q.-Y. Fan, Y. Liu, A. Zhang, Z. Li, Y. Hao, L. Chen, F. Liu, X. Gu, S. Zeng, Discovering surface structure and the mechanism of graphene oxide-triggered CeO_2-WO_3/TiO_2 catalysts for NO abatement with NH_3, ACS Catal. 12 (2022) 8386–8403.
[42] L. Li, L. Zhang, K. Ma, W. Zou, Y. Cao, Y. Xiong, C. Tang, L. Dong, Ultra-low loading of copper modified TiO_2/CeO_2 catalysts for low-temperature selective catalytic reduction of NO by NH_3, Appl. Catal. B: Environ. 207 (2017) 366–375.
[43] X. Yao, R. Zhao, L. Chen, J. Du, C. Tao, F. Yang, L. Dong, Selective catalytic reduction of NO_x by NH_3 over CeO_2 supported on TiO_2: comparison of anatase, brookite, and rutile, Appl. Catal. B: Environ. 208 (2017) 82–93.
[44] Y. Peng, K. Li, J. Li, Identification of the active sites on CeO_2-WO_3 catalysts for SCR of NO_x with NH_3: an in situ IR and Raman spectroscopy study, Appl. Catal. B: Environ. 140–141 (2013) 483–492.
[45] B.B. Burton, S.W. Kang, S.W. Rhee, S.M. George, SiO_2 Atomic layer deposition using tris(dimethylamino)silane and hydrogen peroxide studied by *in situ* transmission FTIR spectroscopy, J. Phys. Chem. C 113 (2009) 8249–8257.
[46] G. Ranga Rao, Z.-H. Wang, H. Watanabe, M. Aoyagi, T. Urisu, A comparative infrared study of H_2O reactivity on Si(1 0 0)-(2 × 1), (2 × 1)-H, (1 × 1)-H and (3 × 1)-H surfaces, Surf. Sci. 570 (2004) 178–188.
[47] S. Xie, W. Tan, Y. Li, L. Ma, S.N. Ehrlich, J. Deng, P. Xu, F. Gao, L. Dong, F. Liu, Copper single atom-triggered niobia-ceria catalyst for efficient low-temperature reduction of nitrogen oxides, ACS Catal. 12 (2022) 2441–2453.
[48] F. Liu, W. Shan, Z. Lian, J. Liu, H. He, The smart surface modification of Fe_2O_3 by WO for significantly promoting the selective catalytic reduction of NO with NH_3, Appl. Catal. B: Environ. 230 (2018) 165–176.
[49] S. Tamm, N. Vallim, M. Skoglundh, L. Olsson, The influence of hydrogen on the stability of nitrates during H_2-assisted SCR over Ag/Al_2O_3 catalysts - a DRIFT study, J. Catal. 307 (2013) 153–161.